

Baseline optimization for the measurement of CP violation, mass hierarchy, and θ_{23} octant in a long-baseline neutrino oscillation experiment

M. Bass,³ M. Bishai,² D. Cherdack,³ M. Diwan,² Z. Djurcic,¹ J. Hernandez,⁵ B. Lundberg,⁴
V. Paolone,⁶ X. Qian,² R. Rameika,⁴ L. Whitehead,⁵ R.J. Wilson,³ E. Worcester,² and G. Zeller⁴

¹Argonne National Lab., Argonne, IL 60439, USA

²Brookhaven National Lab., Upton, NY 11973-5000, USA

³Colorado State University, Fort Collins, CO 80523, USA

⁴Fermi National Accelerator Lab., Batavia, IL 60510-0500, USA

⁵Univ. of Houston, Houston, Texas, 77204, USA

⁶Univ. of Pittsburgh, Pittsburgh, PA 15260, USA

(Dated: February 26, 2015)

Next-generation long-baseline electron neutrino appearance experiments will seek to discover CP violation, determine the mass hierarchy and resolve the θ_{23} octant. In light of the recent precision measurements of θ_{13} , we consider the sensitivity of these measurements in a study to determine the optimal baseline, including practical considerations regarding beam and detector performance. We conclude that a detector at a baseline of at least 1000 km in a wide-band muon neutrino beam is the optimal configuration.

PACS numbers: 14.60.Pq

I. INTRODUCTION

The goals of next-generation neutrino experiments include searching for CP violation in the lepton sector and precision studies of the neutrino mixing matrix. These measurements require an optimal combination of the experimental baseline (the distance between the neutrino source and detector) and the neutrino beam energy. In this paper, we study the baseline optimization for a long-baseline neutrino experiment, assuming a wide-band neutrino beam originating from the Fermilab proton complex.

Experimental observations [1–11] have shown that neutrinos have mass and undergo flavor oscillations due to mixing between the mass states and flavor states. For three neutrino flavors, the mixing can be described by three mixing angles (θ_{12} , θ_{13} , θ_{23}) and one CP-violating phase parameter (δ_{CP}). The probability for flavor os-

cillations also depends on the differences in the squared masses of the neutrinos, Δm_{21}^2 and Δm_{31}^2 , where $\Delta m_{ij}^2 \equiv m_i^2 - m_j^2$ and $\Delta m_{31}^2 = \Delta m_{32}^2 + \Delta m_{21}^2$.

Five of the parameters governing neutrino oscillations have been measured: all three mixing angles and the magnitude of the two independent mass squared differences. Because the sign of Δm_{31}^2 is not known, there are two possibilities for the ordering of the neutrino masses, called the mass hierarchy: $m_1 < m_2 < m_3$ (“normal hierarchy”) or $m_3 < m_1 < m_2$ (“inverted hierarchy”). The value of the CP-violating phase δ_{CP} is unknown. Another remaining question is the octant of θ_{23} : measured values of $\sin^2(2\theta_{23})$ are close to 1 [1, 3, 5], but the data are so far inconclusive as to whether θ_{23} is less than or greater than 45° , the value for maximal mixing between ν_μ and ν_τ .

The mass hierarchy, the value of δ_{CP} , and the θ_{23} octant (value of $\sin^2 \theta_{23}$) affect the muon neutrino to electron neutrino oscillation probability over a long baseline. The oscillation probability can be approximated by [12]

$$\begin{aligned}
 P(\nu_\mu \rightarrow \nu_e) \approx & \sin^2 \theta_{23} \sin^2 2\theta_{13} \frac{\sin^2(\Delta_{31} - aL)}{(\Delta_{31} - aL)^2} \Delta_{31}^2 \\
 & + \sin 2\theta_{23} \sin 2\theta_{13} \sin 2\theta_{12} \frac{\sin(\Delta_{31} - aL)}{(\Delta_{31} - aL)} \Delta_{31} \frac{\sin(aL)}{(aL)} \Delta_{21} \cos(\Delta_{31} + \delta_{CP}) \\
 & + \cos^2 \theta_{23} \sin^2 2\theta_{12} \frac{\sin^2(aL)}{(aL)^2} \Delta_{21}^2
 \end{aligned} \tag{1}$$

where $\Delta_{ij} = \Delta m_{ij}^2 L / 4E_\nu$, $a = G_F N_e / \sqrt{2}$, G_F is the Fermi constant, N_e is the number density of electrons in the Earth, L is the baseline in km, and E_ν is the neutrino energy in GeV. The corresponding probability

for antineutrinos is the same, except that $a \rightarrow -a$ and $\delta_{CP} \rightarrow -\delta_{CP}$. Figure 1 shows the probability as a function of L/E_ν for various cases.

The maximum oscillation probabilities in vacuum oc-

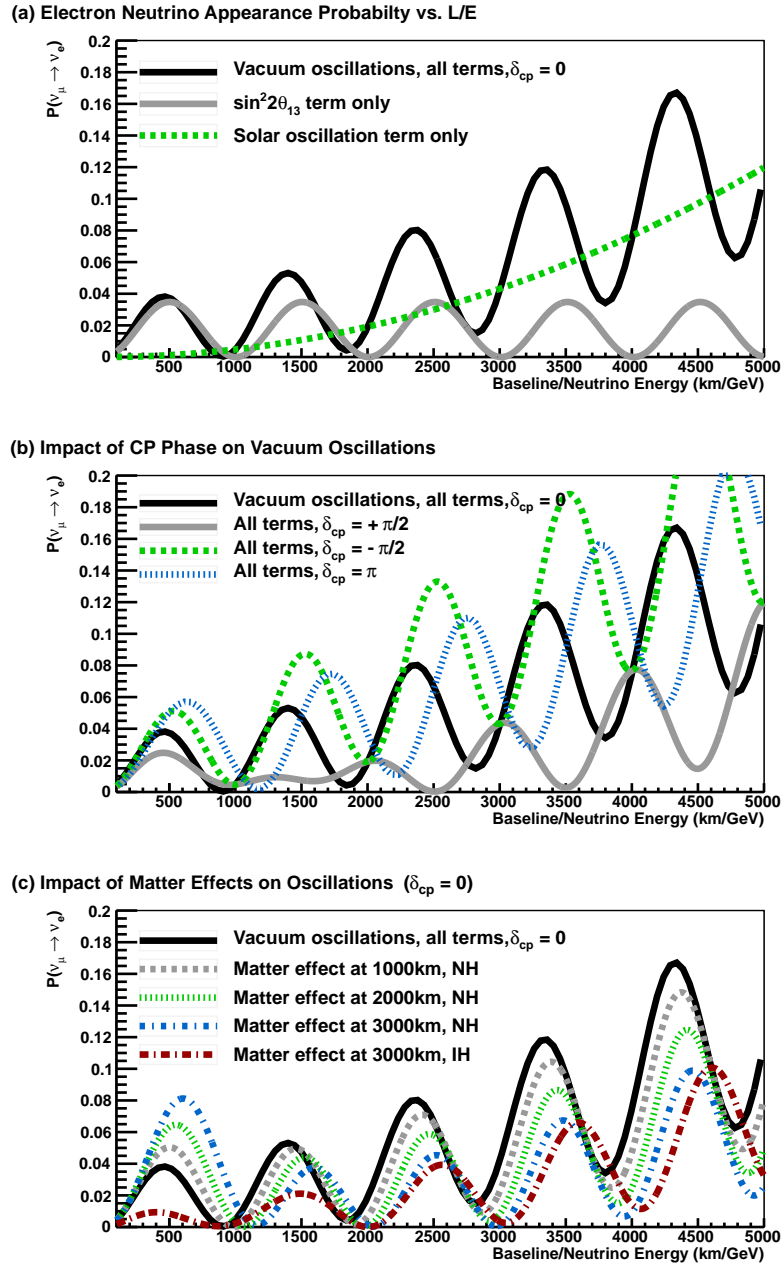


FIG. 1. The $\nu_\mu \rightarrow \nu_e$ oscillation probability as a function of baseline/neutrino energy (L/E_ν) as given by Equation 1. The top graph (a) shows the full probability for vacuum oscillations with $\delta_{CP} = 0$ and shows the contribution from the $\sin^2(2\theta_{13})$ term and the $\sin^2(2\theta_{12})$ term (also called the solar term). The middle graph (b) shows the full probability in vacuum for different values of δ_{CP} . The bottom graph (c) shows the full probability in matter, assuming constant matter density, for different baselines compared to the vacuum probability with $\delta_{CP} = 0$. The oscillation parameter values used to draw these curves are given in Section IV.

cur at

$$\frac{L}{E_n} \left(\frac{\text{km}}{\text{GeV}} \right) \approx (2n - 1) \left(\frac{\pi}{2} \right) \frac{1}{1.267 \times \Delta m_{32}^2 (\text{eV}^2)}, \quad (2)$$

where E_n is the neutrino energy at the n^{th} oscillation maximum. For longer baselines, it is possible to observe multiple oscillation maxima in the spectra if the neutrino

flux covers a wide range of energy. At short baselines, the higher order maxima ($n > 1$) are typically too low in energy to be observable with high-energy accelerator beams.

A CP-violating value of δ_{CP} ($\delta_{CP} \neq 0$ and $\delta_{CP} \neq \pi$) would cause a difference in the probabilities for $\nu_\mu \rightarrow \nu_e$ and $\bar{\nu}_\mu \rightarrow \bar{\nu}_e$ transitions. The CP asymmetry \mathcal{A}_{cp} is

defined as

$$\mathcal{A}_{cp}(E_\nu) = \frac{P(\nu_\mu \rightarrow \nu_e) - P(\bar{\nu}_\mu \rightarrow \bar{\nu}_e)}{P(\nu_\mu \rightarrow \nu_e) + P(\bar{\nu}_\mu \rightarrow \bar{\nu}_e)}. \quad (3)$$

If $\delta_{CP} = 0$ or π , the transition probability for oscillations in vacuum is the same for neutrinos and antineutrinos. For oscillations in matter, the MSW matter effect [13, 14] creates a difference between the neutrino and antineutrino probabilities, even for $\delta_{CP} = 0$ or $\delta_{CP} = \pi$. For oscillations in matter with $\delta_{CP} \neq 0$ and $\delta_{CP} \neq \pi$, there is an asymmetry due to both CP violation and the matter effect. A leading-order approximation of the CP asymmetry in the three-flavor model is given by [15]

$$\mathcal{A}_{cp}(E_\nu) \approx \frac{\cos \theta_{23} \sin 2\theta_{12} \sin \delta_{CP}}{\sin \theta_{23} \sin \theta_{13}} \left(\frac{\Delta m_{21}^2 L}{4E_\nu} \right) + \text{matter effects}. \quad (4)$$

In principle, a measurement of the parameter δ_{CP} could be performed based on a spectrum shape fit with only neutrino beam data. However, long-baseline experiments seek not only to measure the parameter, but to explicitly demonstrate CP violation by observing the asymmetry between neutrinos and antineutrinos. Additionally, a comparison of the measured value of δ_{CP} based on neutrino data alone to that based on the combined fit of neutrino and antineutrino data will be a useful cross-check.

Figure 2 shows the asymmetry for different baselines calculated at both the first and second oscillation maxima, since only these two maxima are accessible in practical accelerator experiments. The asymmetry is shown assuming only matter effects ($\delta_{CP} = 0$) or only maximal δ_{CP} effects (in vacuum). The matter asymmetry grows as a function of baseline, and therefore distinguishing the normal and inverted hierarchies by measuring neutrino and antineutrino events becomes easier as the baseline increases, as long as the number of appearance events stays constant. The asymmetry due to nonzero δ_{CP} is constant as a function of baseline at both the first and second oscillation maximum. At the first oscillation maximum, the maximum CP asymmetry is larger than the matter asymmetry only for baselines less than ~ 1000 km. However, at the second oscillation maximum, the maximal CP asymmetry dominates the matter asymmetry at all baselines. The second oscillation maximum therefore has good sensitivity to CP violation, independent of the

mass hierarchy. At short baselines, the second oscillation maximum occurs at an energy that isn't observable. Therefore at short baselines, any observed asymmetry could be due to either the matter effect or CP violation at the first oscillation maximum; additional information is needed to determine the cause of the asymmetry. At longer baselines with a wide-band beam, the ambiguity at the first oscillation maximum can be resolved using the information from the second oscillation maximum.

Previous studies (for example, [16–18]) have considered the optimal baseline for measurements of muon neutrino to electron neutrino oscillations using a wide-band neutrino beam from Fermilab. However, these studies were conducted before the value of θ_{13} was measured by reactor antineutrino experiments [9–11]. The measured value of θ_{13} has been incorporated into other recent long-baseline oscillation sensitivity estimates, but the study presented in this paper is unique in considering different baselines. We reconsider the baseline optimization for an electron neutrino appearance measurement using the measured value of θ_{13} and realistic simulations of a wide-band neutrino beam facility at Fermilab.

II. EXPECTED ELECTRON NEUTRINO APPEARANCE RATE

In a conventional neutrino beam, protons hit a stationary target producing secondary particles, most of which are pions. The positively charged pions are focused in the forward direction by a toroidal magnetic field generated by magnetic horns. The pions are then allowed to decay to produce a muon neutrino beam. At the end of the decay region an absorber stops the remaining secondary particles from the initial proton collision, and the muons produced in the decay pipe are stopped in rock located beyond the absorber. A muon antineutrino beam can be created by reversing the magnetic field to focus negatively charged pions. Horn-focused beams are technologically well-matched to long-baseline experiments with neutrino energy > 1 GeV since horn focusing is optimal for focusing hadrons > 2 GeV and can be used effectively to charge-select the focused hadrons. In this study, we use the simulated flux from horn-focused beams to evaluate the sensitivity of long-baseline neutrino oscillation experiments at different baselines. In this section, we discuss the expected dependence of the electron neutrino appearance rate on baseline, making ideal flux assumptions and ignoring any detector effects for simplicity.

The total number of electron neutrino appearance events expected for a given exposure from a muon neutrino source as a function of baseline is given as

$$N_{\nu_e}^{\text{appear}}(L) = N_{\text{target}} \int \Phi^{\nu_\mu}(E_\nu, L) \times P^{\nu_\mu \rightarrow \nu_e}(E_\nu, L) \times \sigma^{\nu_e}(E_\nu) dE_\nu \quad (5)$$

where $\Phi^{\nu_\mu}(E_\nu, L)$ is the muon neutrino flux as a function of neutrino energy, E_ν , and baseline, L , $\sigma^{\nu_e}(E_\nu)$ is the electron neutrino inclusive charged-current cross-section per nucleon (N), N_{target} is the number of target nucleons per

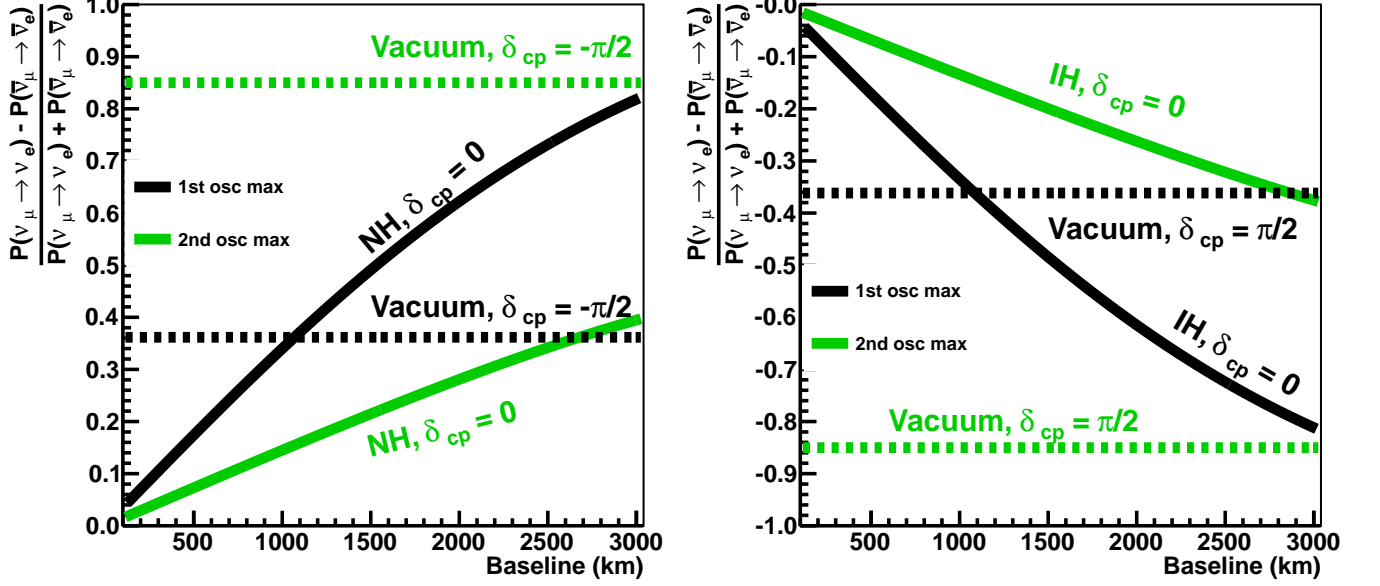


FIG. 2. Asymmetry vs baseline at the first (black line) and second (green line) oscillation maxima. The solid lines show the asymmetry due to the matter effect only ($\delta_{CP} = 0$) for the normal hierarchy (left plot) or inverted hierarchy (right plot). The dashed lines show the maximum CP asymmetry in vacuum, with $\delta_{CP} = -\pi/2$ (left plot) or $\delta_{CP} = \pi/2$ (right plot). The oscillation parameter values used to draw these curves are given in Section IV.

kt of detector fiducial volume, and $P^{\nu_\mu \rightarrow \nu_e}(E_\nu, L)$ is the appearance probability in matter. For this discussion, the units are always assumed to be km for L , GeV for E_ν , and eV^2 for Δm_{31}^2 .

For a simple estimate of the electron neutrino appearance rate as a function of baseline, we assume the neutrino beam source produces a flux that is constant in the oscillation energy region (Equation 6), and we approximate the appearance probability with the dominant term without matter effects (Equation 7). The expressions for the electron neutrino charged-current cross-section and number of target nucleons per kt are given in Equations 8 and 9, respectively.

$$\Phi^{\nu_\mu}(E_\nu, L) \approx \frac{C}{L^2}, \quad C = \text{number of } \nu_\mu/\text{m}^2/\text{GeV}/(\text{MW}\cdot\text{yr}) \text{ at } 1 \text{ km} \quad (6)$$

$$P^{\nu_\mu \rightarrow \nu_e}(E_\nu, L) \approx \sin^2 \theta_{23} \sin^2 2\theta_{13} \sin^2(1.27\Delta m_{31}^2 L/E_\nu) \quad (7)$$

$$\sigma^{\nu_e}(E_\nu) = 0.67 \times 10^{-42} (\text{m}^2/\text{GeV}/N) \times E_\nu, \quad E_\nu > 0.5 \text{ GeV} \quad (8)$$

$$N_{\text{target}} = 6.022 \times 10^{32} N/\text{kt} \quad (9)$$

For a 120-GeV proton beam from the Fermilab Main Injector with a live time of 2×10^7 s/yr, 1 MW-yr corresponds to approximately 10^{21} protons on target. A beam simulation with perfect hadron focusing (in which all secondary mesons are assumed to be focused towards the far detector) produces a peak flux of roughly $0.12 \times 10^{-3} \nu_\mu/\text{m}^2/\text{GeV}/\text{proton-on-target}$ at 1 km (see Figure 5). Combining these numbers and naively assuming a flat spectrum, we obtain $C \approx 1.2 \times 10^{17} \nu_\mu/\text{m}^2/\text{GeV}/(\text{MW}\cdot\text{yr})$ at 1 km. Using this assumption and the approximations in Equations 6-9, we find that

$$N_{\nu_e}^{\text{appear}}(L) \approx (1.8 \times 10^6 \text{ events}/(\text{kt}\cdot\text{MW}\cdot\text{yr}))(\text{km}/\text{GeV})^2 \times \int_{x_0}^{x_1} \frac{\sin^2(ax)}{x^3} dx, \quad (10)$$

$$x \equiv L/E_\nu, \quad a \equiv 1.27\Delta m_{31}^2.$$

Integrating Equation 10 over the region of the first two oscillation maxima such that $x_0 = 100 \text{ km}/\text{GeV}$ and $x_1 = 2000 \text{ km}/\text{GeV}$ (see Figure 1), yields

$$N_{\nu_e}^{\text{appear}}(L) \sim \mathcal{O}(20) \text{ events}/(\text{kt}\cdot\text{MW}\cdot\text{yr}) \quad (11)$$

As seen from the simplified discussion presented above, the ν_e appearance rate for vacuum oscillations is a con-

stant that is largely independent of baseline for baselines

>300 km. The event rates at experiments with baselines <300 km are lower because the neutrino cross-sections at energies < 0.5 GeV are not linear with energy. For oscillations in matter, the electron neutrino appearance probability at the first oscillation maximum increases with baseline for the case of normal hierarchy (as shown in Figure 1c) and decreases for inverted hierarchy.

For real neutrino beams generated from pion decays in flight, it is not possible to produce a neutrino flux that is constant over a large range of energies. Hadron production from the proton target and decay kinematics due to the finite decay volume will produce a reduced neutrino flux at higher energies when a fixed proton beam energy is used. The lower flux at higher energies, and hence longer baselines, will counteract the event rate increase from the matter effect (assuming a neutrino beam and normal hierarchy). This effect is illustrated in Figure 3. We calculate the ν_e appearance event rate integrated over the region of the first two oscillation maxima using the appearance probability given by Equation 1 assuming a constant flux or a horn-focused beam with a perfect-focusing system. For the constant flux assumption, we use Equation 6 with $C \approx 1.2 \times 10^{17} \nu_\mu/\text{m}^2/\text{GeV}/(\text{MW}\cdot\text{yr})$ as before. The results from this more detailed calculation are comparable to Equation 11 and illustrate the slowly varying dependence on baseline.

Figure 4 shows separately the event rate in each of the first two oscillation maxima assuming the flux obtained from a perfect-focusing system with a fixed decay pipe length. With perfect focusing, the event rate in the region of the second oscillation maximum is relatively constant for baselines greater than 1200 km. Therefore, based on these considerations, we don't expect the sensitivity to CP violation to increase as a function of baseline, but remain roughly the same. The event rate in the region of the first maximum decreases with baseline due to the decreasing flux from the beam and increasing impact from the matter asymmetry. For longer baselines, the decrease in flux in the region of the first maximum can be ameliorated by using longer decay pipes to increase the number of pion decays at higher energy.

The perfect-focusing system assumed in Figure 4 uses a 120-GeV primary proton beam which can be produced at the Fermilab Main Injector. An alternate strategy of focusing on the second oscillation maximum at long baselines by using a lower primary proton beam energy will not be considered in this study. With a lower proton energy, the integrated rates in the first and second oscillation maxima are more similar, and the second maximum contributes greatly to the CP violation sensitivity. At 120 GeV however, the rates at the first maximum dominate at all baselines in neutrino mode (shown in Figure 4), and accessing the second maximum by going to longer baselines is unlikely to yield significant enhancements to the sensitivity. The optimal baseline therefore depends on the energy of the primary proton beam. The highest power from the Fermilab proton complex is currently available at an energy of 120 GeV, and that is the only

proton beam energy considered in this study.

The sensitivity studies in this paper assume a horn-focused neutrino beam with realistic focusing and include detector effects. The NuMI [19] design of double-parabolic horns was chosen as the basis for these simulations because the NuMI horns were designed to be used as tunable, focusing magnetic lenses over a wide range of hadron energy. The comparison between perfect focusing and focusing using the NuMI system is given in Figure 5, which shows the neutrino flux at 1 km from a 120-GeV proton beam incident on a target two interaction lengths in thickness. An evacuated hadron decay pipe 380 m in length and 4 m in diameter is assumed for this comparison. The next section discusses the details of the simulated fluxes with realistic focusing used for the sensitivity calculations at each baseline.

III. BEAM SIMULATIONS

This study uses neutrino and antineutrino fluxes derived from GEANT3 [20] beamline simulations optimized to cover the energy region of the first oscillation maximum (and the second maximum if possible) at each baseline considered. The beam simulation at each baseline assumes a 1.2-MW 120-GeV primary proton beam that delivers 1×10^{21} protons-on-target per year. A graphite target with a diameter of 1.2 cm and a length equivalent to two interaction lengths is assumed. The double-parabolic NuMI focusing horn design is used [19], with a horn current of 250 kA. The separation between the two horns is assumed to be 6 m. The decay pipe is 4 m in diameter and is assumed to be evacuated. The beamline parameters that are varied for different baselines (distance between target and horn, decay pipe length, and off-axis angle) are summarized in Table I. We change the decay pipe length in increments of 100 m to match the decay length of a pion whose energy corresponds to the neutrino energy of the first oscillation maximum. For baselines > 1000 km, when considering different configurations that cover the oscillation region appropriately, we choose the configuration at each baseline that maximizes CP sensitivity.

Figure 6 shows the ratio of the ν_e appearance signal spectra used in this study (assuming $\delta_{CP} = 0$ and normal hierarchy) to the appearance spectra obtained assuming perfect hadron focusing for baselines of 1000, 2000, and 3000 km. The perfect-focusing fluxes use the same decay pipe lengths for each baseline as given in Table I. The simulated fluxes achieve up to $\sim 80\%$ of the perfect-focusing flux in the region of interest, indicated by the horizontal lines for each spectrum; our calculations are based on the achievable and excellent performance characteristics of such beams.

Because conventional neutrino beams (with currently understood technological limits on magnetic field strengths) are not efficient at focusing hadrons with energy less than 1 GeV, we use off-axis beams to gener-

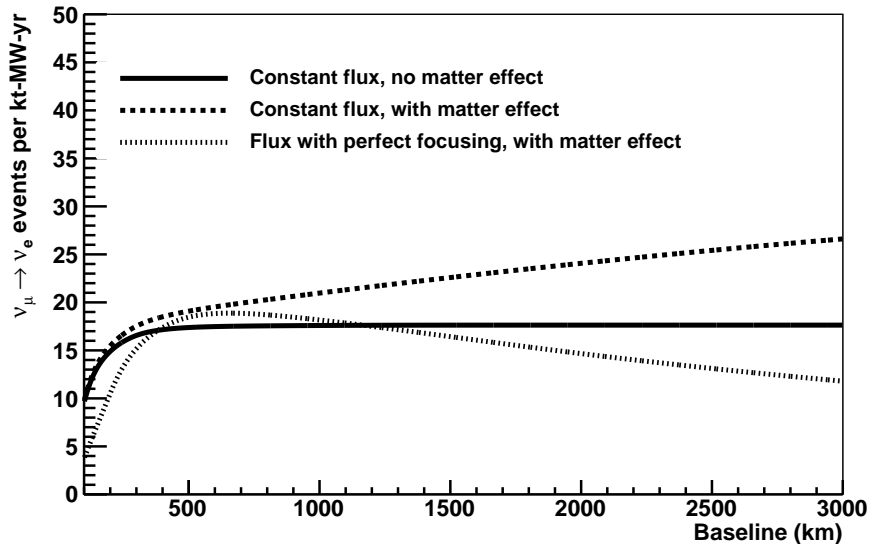


FIG. 3. Estimated ν_e appearance rates (with no detector effects) integrated over the first two oscillation maxima as a function of baseline for three conditions. The solid and dashed lines are the event rates obtained using a neutrino flux that is constant as a function of energy. The solid line assumes oscillations in vacuum and the dashed line assumes oscillations in a constant matter density with normal hierarchy. The dotted-dashed line is the event rate calculation using a neutrino-beam flux obtained from a perfect-focusing system with a 120-GeV primary beam and a fixed decay pipe length of 380 m assuming normal hierarchy.

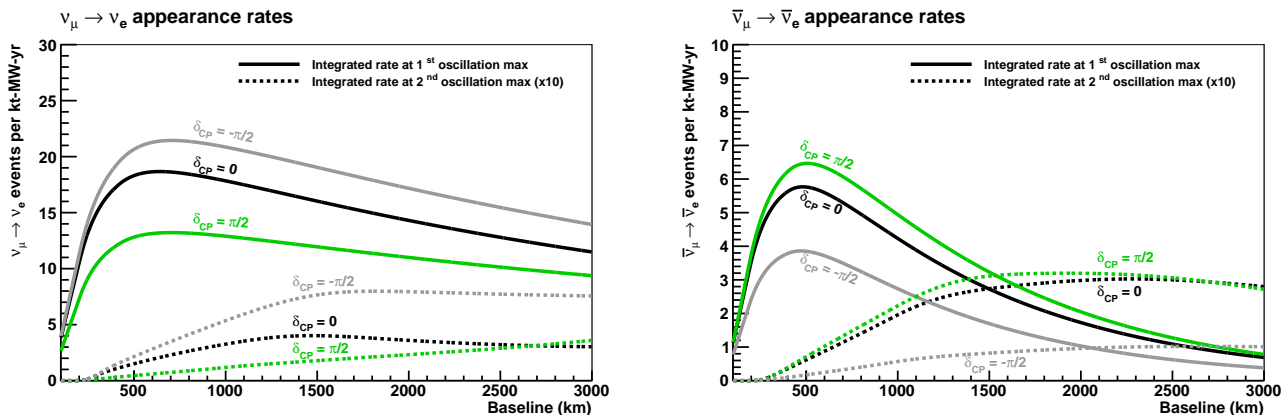


FIG. 4. Estimated ν_e (left) and $\bar{\nu}_e$ (right) appearance rates (with no detector effects) integrated over an energy region around the first oscillation maximum (solid line) or the second oscillation maximum (dashed line) assuming the flux obtained from a perfect-focusing system with a 120-GeV primary beam and a fixed decay pipe length of 380 m. The curves are shown for different values of δ_{CP} . Matter effects are included assuming normal hierarchy. The rates for the second oscillation maximum have been increased by a factor of 10 for visibility.

ate the flux required for baselines shorter than 1000 km. The off-axis beams are tuned to match the energy range of the first oscillation maximum. Studies have indicated that in addition to varying the focusing geometry and off-axis angle, further optimization could be obtained by varying the proton beam energy for the shorter baselines, but the highest power from the Fermilab proton complex is available at an energy of 120 GeV. As a point of comparison, we considered an on-axis beam with an 8-GeV primary proton beam at 300 km with the same ex-

posure and found that the event rate wasn't better than the off-axis 120-GeV beam (580 signal events and 290 total background events integrated in reconstructed energy over the first maximum, to be compared with numbers in Table III).

While further refinements could be made to the flux optimization, the fluxes used in this study are nearly optimal for each baseline and are realistic representations of what could be achieved with a neutrino beam facility at Fermilab.

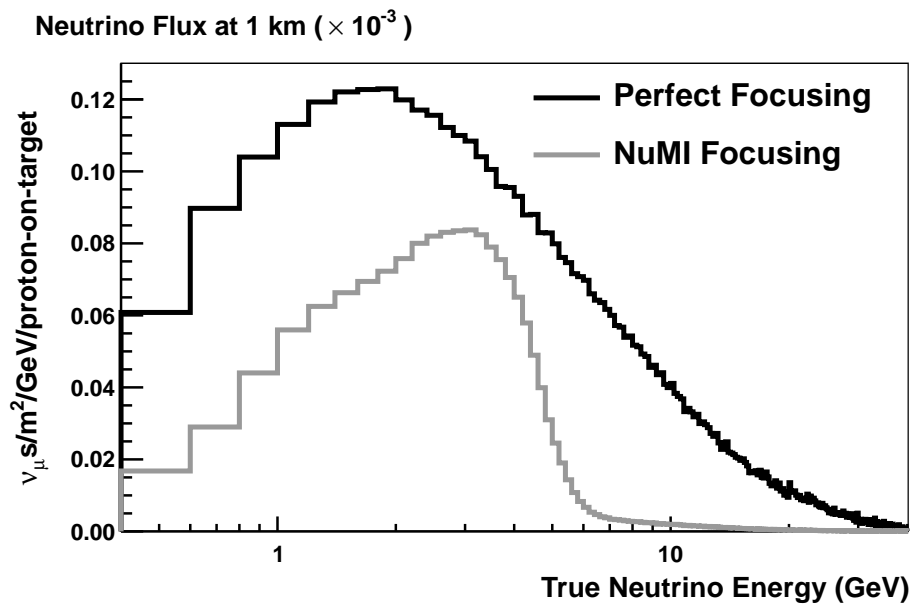


FIG. 5. The neutrino flux at 1 km from a 120-GeV proton beam incident on a target two interaction lengths in thickness. The black histogram is the flux from a perfectly focused hadron beam and a decay pipe 380 m in length. The gray histogram is the flux obtained using the NuMI focusing system operating at a current of 250 kA. (The focusing system works similarly for the antineutrino spectrum.)

TABLE I. The beam configuration used at each baseline to determine the optimal baseline for the next generation long-baseline experiment. The beam parameters are chosen to cover the first oscillation maximum at each baseline.

| Baseline | Target-Horn 1 distance | Decay pipe length | Off-axis angle |
|----------|------------------------|-------------------|----------------|
| 300 km | 30 cm | 280 m | 2° |
| 500 km | 30 cm | 280 m | 1.5° |
| 750 km | 30 cm | 280 m | 1.0° |
| 1000 km | 0 cm | 280 m | 0° |
| 1300 km | 30 cm | 380 m | 0° |
| 1700 km | 30 cm | 480 m | 0° |
| 2000 km | 70 cm | 580 m | 0° |
| 2500 km | 70 cm | 680 m | 0° |
| 3000 km | 100 cm | 780 m | 0° |

IV. EXPERIMENTAL ASSUMPTIONS

The signal of muon (anti)neutrino to electron (anti)neutrino oscillations is an excess of ν_e or $\bar{\nu}_e$ charged-current (CC) interactions over background. ν_e ($\bar{\nu}_e$) CC events are identified by the e^- (e^+) in the final state. An irreducible background is caused by ν_e and $\bar{\nu}_e$ intrinsic to the beam, most of which are created by decays of kaons and muons in the decay region. Neutral-current (NC) interactions create background when the hadronic shower has an electromagnetic component, often caused by the decay of π^0 s. ν_μ CC interactions create background when the final state muon is not identified. Due to $\nu_\mu \rightarrow \nu_\tau$ oscillations, there is background contribution from ν_τ CC interactions in which the decay products of the τ mimic a signal event. We expect that additional kinematic cuts

can be applied to the selected sample to reduce the background from ν_τ CC interactions without a significant loss of signal events. In this study we consider two cases: the maximum ν_τ CC background assuming no background reduction is possible and zero ν_τ CC background assuming it can be completely eliminated with no reduction in signal. The ν_τ CC background is most important for the longer baseline configurations (>1500 km), in which a significant portion of the neutrino flux has energy above the τ production threshold.

In the neutrino-beam mode, there is a small background from wrong-sign (antineutrino) contamination in the beam, which we consider negligible. However, in the antineutrino-beam mode, the wrong-sign (neutrino) contamination is much more substantial, and is therefore included in this study.

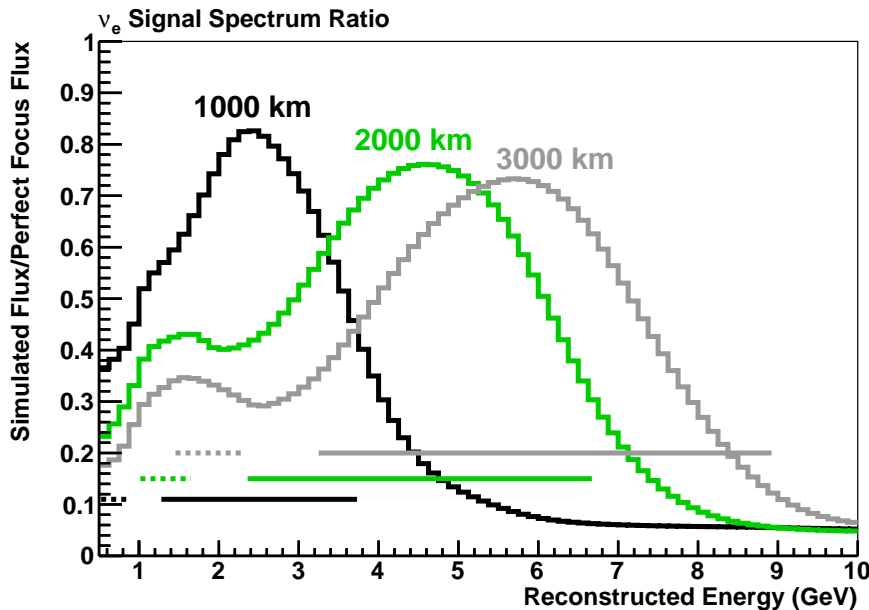


FIG. 6. Ratio of the ν_e appearance signal spectra used in this study to the appearance spectra obtained assuming perfect hadron focusing for baselines of 1000, 2000, and 3000 km. The solid horizontal lines show the energy region around the first maximum, where the limits are the energies above and below the first maximum at which the appearance probability is 50% of the maximum. The dashed horizontal lines show the energy region around the second maximum, where the limits are the energies above and below the second maximum at which the appearance probability is 10% of the maximum.

TABLE II. Detector performance parameters related to the identification of ν_e CC events.

| Parameter | Value |
|---------------------------------------|-----------------------------|
| ν_e CC efficiency | 80% |
| NC mis-identification rate | 1% |
| ν_μ CC mis-identification rate | 1% |
| ν_τ CC mis-identification rate | $\sim 20\%$ |
| Other background | 0% |
| ν_e CC energy resolution | $15\%/\sqrt{E(\text{GeV})}$ |

As a reference, we use a liquid argon (LAr) TPC with an exposure of 350 kt-MW-yr (which roughly corresponds to a 6-year exposure of a 50-kt detector in a 1.2-MW beam). Our results, however, can be easily extrapolated to other combinations of detector size and beam intensity. Parameters describing the selection efficiency and detector energy response were input into the GLOBES software package [21, 22] to calculate and analyze the predicted spectra. The detector performance parameters used for the study are shown in Table II. Most of these parameters are derived from studies of LAr TPC simulations and studies of the ICARUS detector performance [23–26]. The NC true-to-visible energy conversion is based on a fast MC simulation developed for LBNE [27, 28], a planned experiment which will use a muon neutrino beam to study electron neutrino appearance. The MC uses flux simulations (derived from GEANT3

beamline simulations as previously described) and the GENIE event generator [29] to generate neutrino interactions on argon. Events can be classified as ν_e CC-like based on event-level reconstructed quantities. The ν_τ CC background energy-dependent mis-identification rate and true-to-visible energy conversion is also calculated based on the fast MC.

The oscillation parameter values and uncertainties assumed in this study are: $\theta_{12} = 34 \pm 1^\circ$, $\theta_{13} = 9 \pm 1^\circ$, $\theta_{23} = 38 \pm 3^\circ$ ($\theta_{23} = 52 \pm 3^\circ$ when the second octant solution is considered), $\Delta m_{21}^2 = (7.54 \pm 0.24) \times 10^{-5} \text{ eV}^2$ and $|\Delta m_{31}^2| = (2.47 \pm 0.08) \times 10^{-3} \text{ eV}^2$, mostly based on the global fit in [30]. The uncertainty on θ_{13} comes from the systematic uncertainty given in [31], on the assumption that the statistical uncertainty on θ_{13} will be negligible within a few years. The oscillation probability calculation in GLOBES is exact, and matter effects

are incorporated in GLOBES assuming a constant matter density equal to the average matter density from the PREM [32, 33] onion shell model of the earth. Using the PREM matter profile built into GLOBES rather than the average matter density produces a negligible change in the oscillation signal rates (at most 1%).

The expected neutrino and antineutrino spectra at each baseline are shown in Figures 7-10. The expected event rates, assuming normal hierarchy, for neutrino and antineutrino-beam modes are shown in Tables III and IV, respectively. Figure 11 shows the rates as a function of baseline.

The neutrino signal event rates with realistic flux simulation and detector effects are roughly constant across the baselines considered in the study (Figure 11). The antineutrino rates are lower than the neutrino rates due to both lower π^- production rates and lower antineutrino cross-sections. The antineutrino signal rate decreases slightly with baseline due to the energy dependence of the π^- production, which has a steeper drop-off in energy than the π^+ production rate.

V. ANALYSIS

To compare the sensitivity at each baseline, we use GLOBES to calculate the significance of the mass hierarchy, CP violation, and octant determination. Predicted neutrino and antineutrino spectra are generated for appropriate values of δ_{CP} and the mass hierarchy for the hypothesis being tested, and a χ^2 minimization is performed on the spectra. The χ^2 minimization takes correlations between the oscillation parameters into account and considers both octant solutions for θ_{23} in the mass hierarchy and CP violation analysis. The χ^2 is given by

$$\begin{aligned} \chi^2(\mathbf{n}^{true}, \mathbf{n}^{test}, f) \\ = 2 \sum_i^{N_{reco}} (n_i^{true} \ln \frac{n_i^{true}}{n_i^{test}(f)} + n_i^{test}(f) - n_i^{true}) + f^2 \end{aligned} \quad (12)$$

where \mathbf{n} are the event rate vectors in N_{reco} bins of reconstructed neutrino energy and f is a nuisance parameter to be profiled. The nuisance parameters include the already-measured oscillation parameters and signal and background normalizations. The oscillation parameters are constrained within their experimental uncertainties given in Section IV. We perform a combined fit to the ν_e appearance and ν_μ disappearance spectra. We assume a 1% (5%) uncertainty in the signal normalization for ν_e (ν_μ) and a 5% (10%) uncertainty in the background normalization for ν_e (ν_μ) in the fit, where the normalization uncertainties are uncorrelated among the four ($\nu_e, \bar{\nu}_e, \nu_\mu, \bar{\nu}_\mu$) modes. Achieving this level of precision will require a well-designed near detector and careful analysis of detector efficiencies and other systematic errors. See [27] for a detailed discussion of the expected systematic

uncertainties based on current and former experiments. We will not analyze this issue in this paper.

For the calculations at each baseline, we assume an equal amount of exposure in neutrino-beam mode and antineutrino-beam mode. The relative amount of neutrino and antineutrino beam time could be optimized for each baseline in future studies. For example, it is slightly more optimal at longer baselines to collect more neutrino (antineutrino) data assuming normal mass hierarchy (inverted mass hierarchy).

A. Mass Hierarchy

To calculate the mass hierarchy significance, the χ^2 minimization considers only those solutions that have the opposite hierarchy from that which was used to generate the true spectra. For example, if the true hierarchy is assumed to be normal, we assume the inverted hierarchy for the observed spectra in the χ^2 calculation. This allows us to determine the significance at which we can exclude the inverted hierarchy given the true hierarchy is normal.

To properly interpret the mass hierarchy physics sensitivity, special attention should be paid, as the mass hierarchy determination has only two possible outcomes (normal vs. inverted hierarchy). Ref. [34] carefully examines the statistical nature of this problem and shows the connection between an expected average $\Delta\chi^2$ and probability of mass hierarchy determination. In particular, an experiment with physics sensitivities determined by $\Delta\chi^2 = 9$ and 25 (corresponding to 3 and 5- σ of average separation between the two hypotheses) would have 93.32% and 99.38% probabilities of rejecting the wrong mass hierarchy, with a 6.68% and 0.62% probability of incorrect identification, respectively.

Figure 12 (13) shows the fraction of all possible true δ_{CP} values for which we can determine normal or inverted hierarchy with a minimum value of $\Delta\chi^2 = 9$ (25) as a function of baseline. We find the mass hierarchy can be determined for 100% of all δ_{CP} values at a baseline of at least 1000 km (1300 km) with a minimum value of $\Delta\chi^2 = 9$ (25). The inclusion of the maximum ν_τ CC background does not have a noticeable effect on the mass hierarchy sensitivity. The shaded band shows the possible range in the fraction due to the uncertainty in the other oscillation parameters, dominated by the uncertainty in θ_{23} . Both octant solutions for θ_{23} are considered by the shaded region.

Existing electron neutrino appearance experiments ([6, 35]) and proposed reactor antineutrino experiments [36] will seek to constrain the mass hierarchy before a next-generation long-baseline experiment such as LBNE begins taking data. However, unambiguous determination of the mass hierarchy for all possible values of δ_{CP} is very difficult for existing electron neutrino appearance experiments because of the degeneracy between the matter and CP asymmetries. The electron neutrino appearance and reactor antineutrino disappearance methods are

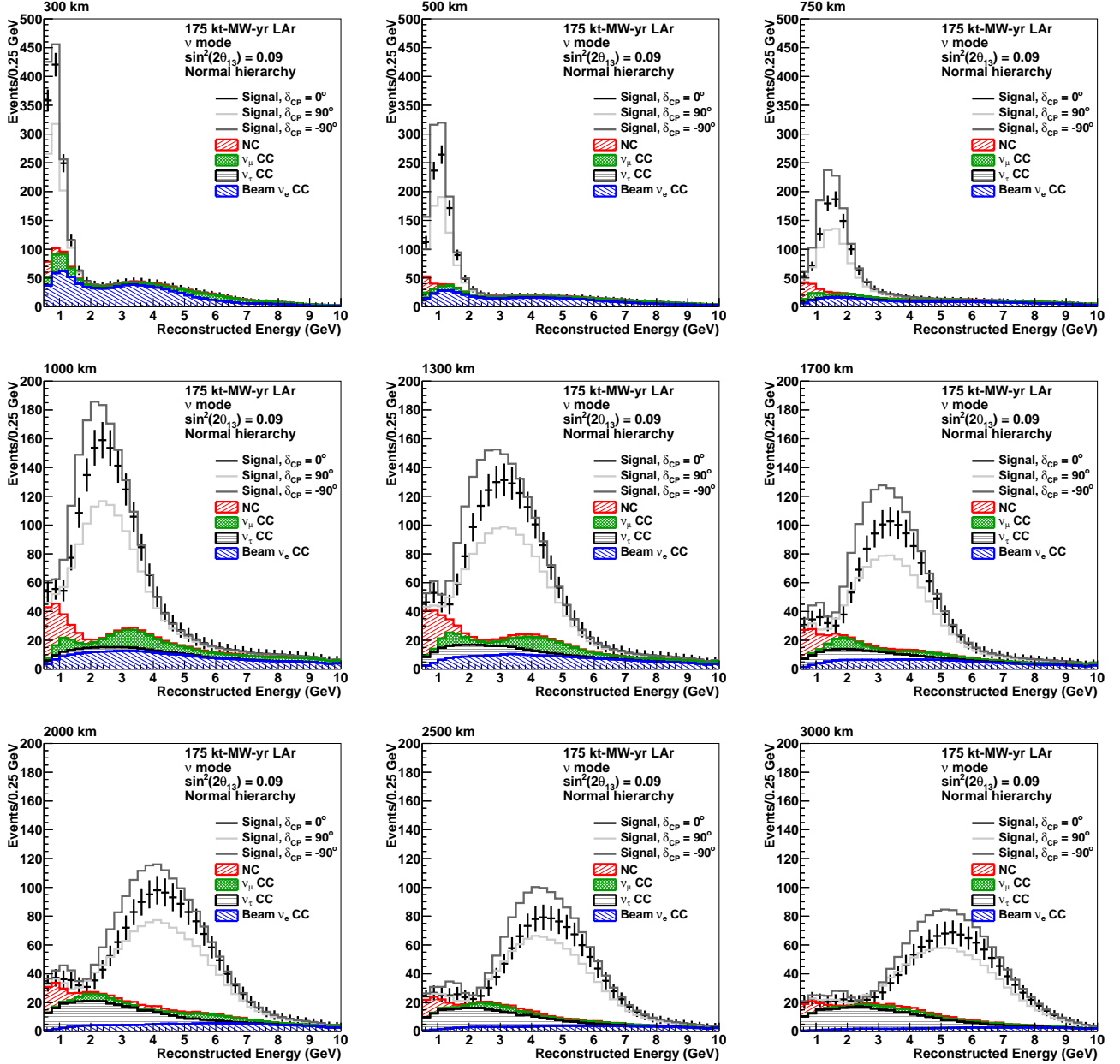


FIG. 7. Neutrino spectra for normal hierarchy: Reconstructed energy distribution of selected ν_e CC-like events assuming a 175 kt-MW-yr exposure in the neutrino-beam mode at each baseline. The plots assume normal mass hierarchy. The signal contribution is shown for various values of δ_{CP} .

complementary, so it is preferable to make both measurements. Therefore, the mass hierarchy sensitivity is still a relevant consideration in choosing the optimal baseline.

The sensitivity calculations above assume a 350 kt-MW-yr exposure. Figure 14 (15) shows the exposure required to determine normal (left) or inverted (right) mass hierarchy with a significance of $\overline{\Delta\chi^2} = 25$ ($\Delta\chi^2 = 9$) for all possible values of δ_{CP} as a function of baseline.

B. CP Violation

To determine the sensitivity to CP violation, we calculate the significance of excluding the CP-conserving values of $\delta_{CP} = 0, \pi$. The significance of the CP violation measurement is defined as $\sigma = \sqrt{\Delta\chi^2}$. Figure 16 shows the fraction of all possible true δ_{CP} values for which we can exclude CP-conserving values of δ_{CP} with a sensitivity of at least 3σ ($\Delta\chi^2 = 9$) as a function of baseline, for both normal and inverted hierarchy. In these plots we assume that the true hierarchy is unknown by considering

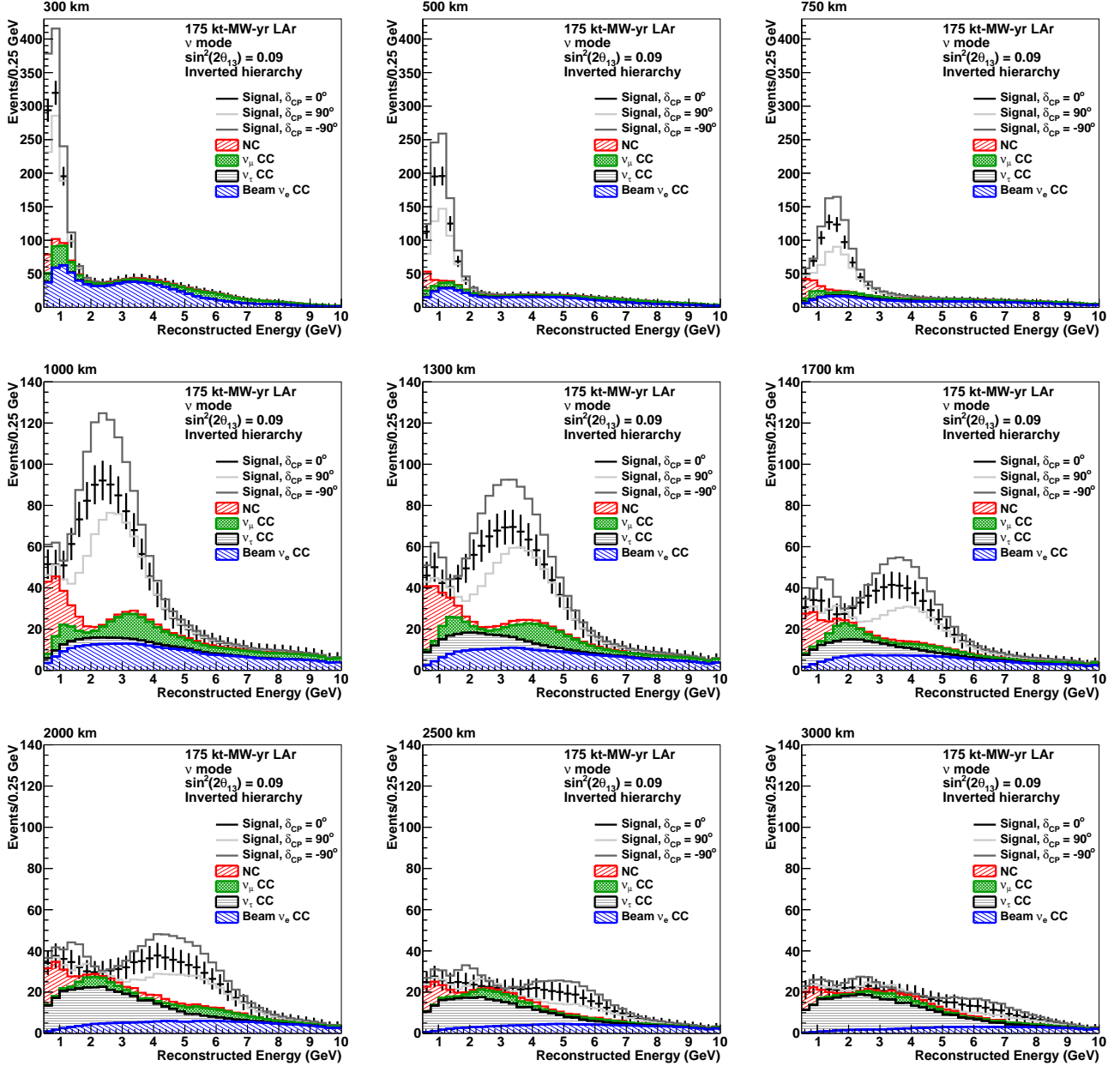


FIG. 8. Neutrino spectra for inverted hierarchy: Reconstructed energy distribution of selected ν_e CC-like events assuming a 175 kt-MW-yr exposure in the neutrino-beam mode at each baseline. The plots assume inverted mass hierarchy. The signal contribution is shown for various values of δ_{CP} .

both hierarchy solutions in the minimization. The maximum sensitivity to CP violation is achieved for baselines between 750 km and 1500 km, with the very short baselines having the worst sensitivity. If the maximum ν_τ CC background is included, the sensitivity decreases for very long baselines. The shaded band shows the possible range in the fraction due to the uncertainty in the other oscillation parameters, dominated by the uncertainty in θ_{23} . Both octant solutions for θ_{23} are considered by the shaded region.

Figure 17 shows CP violation sensitivities in plots sim-

ilar to Figure 16, in which we assume that the true hierarchy is known and consider only those solutions corresponding to the true hierarchy in the minimization. Knowing the mass hierarchy significantly increases the CP violation sensitivity at shorter baselines. This effect is illustrated in Figure 18, which shows the significance as a function of the true value of δ_{CP} for 300 km, 750 km, and 1300 km baselines. The shorter baselines do not have the advantage of the large CP asymmetry in the second oscillation maximum and therefore the CP measurement at short baselines suffers from the ambigu-

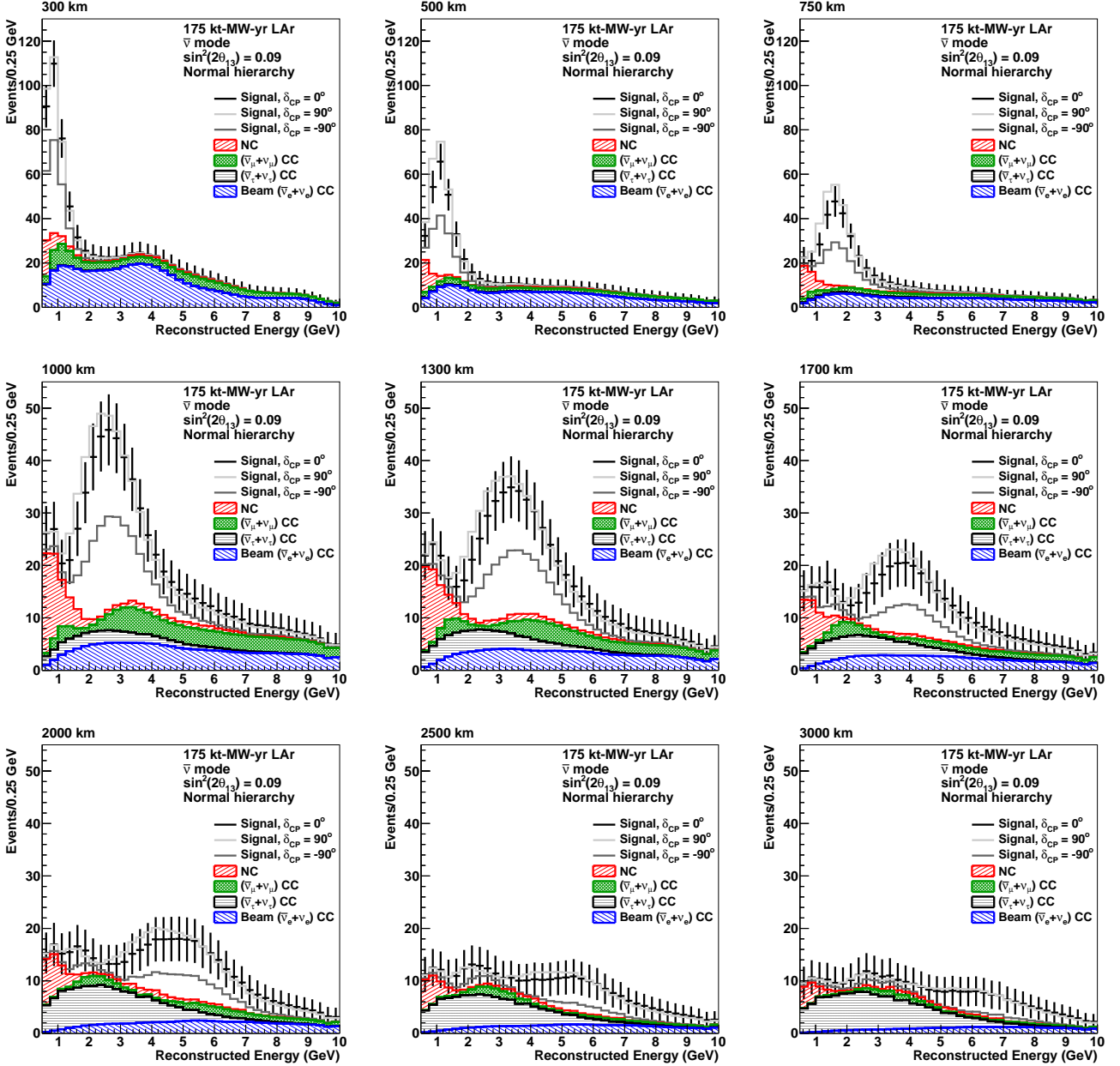


FIG. 9. Antineutrino spectra for normal hierarchy: Reconstructed energy distribution of selected ν_e and $\bar{\nu}_e$ CC-like events assuming a 175 kt-MW-yr exposure in the antineutrino-beam mode at each baseline. The plots assume normal mass hierarchy. The signal contribution is shown for various values of δ_{CP} .

ity of the matter asymmetry and the CP asymmetry in the first oscillation maximum. If the hierarchy is known, this ambiguity is removed. The differences in sensitivity among the baselines are smaller when the mass hierarchy is known, but, as noted in the previous section, an unambiguous measurement of the mass hierarchy using electron neutrino appearance will remain a high priority.

The sensitivity calculations above assume a 350 kt-MW-yr exposure. Figure 19 (20) shows the exposure required to observe CP violation with a significance of 5σ (3σ) for 50% (75%) of all possible values of

δ_{CP} as a function of baseline.

We consider not only the significance of determining CP violation, but also the precision with which the value of δ_{CP} can be measured. Figure 21 shows the δ_{CP} resolution (1σ uncertainty, equivalent to $\Delta\chi^2 = 1$) as a function of baseline for different true values of δ_{CP} . The dependence of the resolution on the value of δ_{CP} is shown explicitly in Figure 22 for different baselines. Figure 23 shows the resolution for each baseline when $\delta_{CP} = 0^\circ$, and compares the resolutions obtained when we include the maximum ν_τ CC background and the range of al-

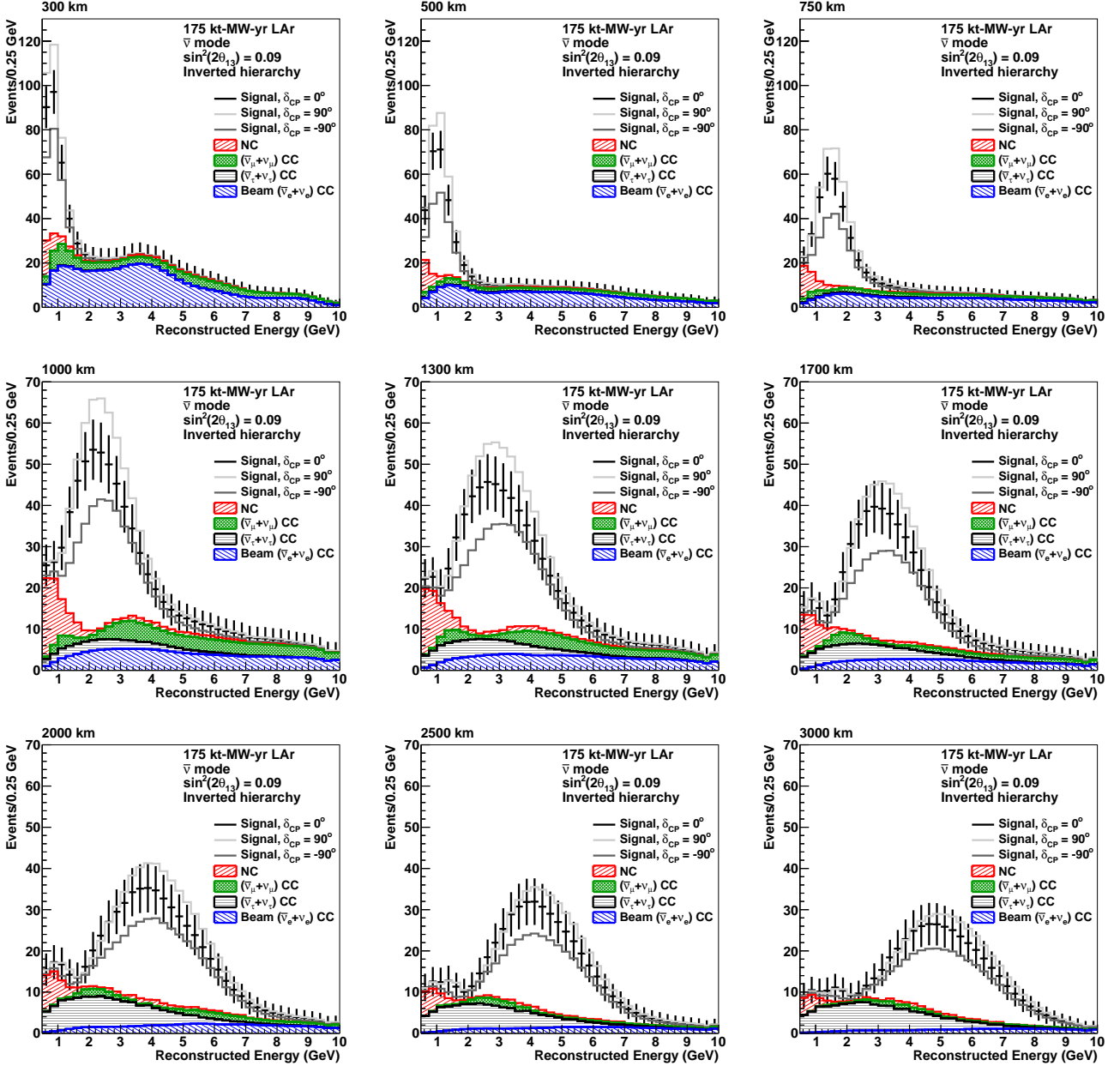


FIG. 10. Antineutrino spectra for inverted hierarchy: Reconstructed energy distribution of selected ν_e and $\bar{\nu}_e$ CC-like events assuming a 175 kt-MW-yr exposure in the antineutrino-beam mode at each baseline. The plots assume inverted mass hierarchy. The signal contribution is shown for various values of δ_{CP} .

lowed values for the oscillation parameters. These plots assume that the mass hierarchy is known. Even if the mass hierarchy is perfectly known, the resolution is poorest for short baselines, particularly for $\delta_{CP} = \pm 90^\circ$ [37]

C. θ_{23} Octant

To calculate the significance of determining the θ_{23} octant, the χ^2 minimization only considers solutions that have the opposite octant from that which is used to gen-

erate the true spectra. For example, if the true value of θ_{23} is assumed to be in the first octant, we assume θ_{23} in the second octant for the observed spectra in the χ^2 calculation. This allows us to determine the significance at which we can exclude the second octant solution given the true value of θ_{23} is in the first octant. The significance of the octant measurement is defined as $\sigma = \sqrt{\Delta\chi^2}$. Figure 24 shows the fraction of all possible true δ_{CP} values for which we can determine the octant with a sensitivity of at least 5σ ($\Delta\chi^2 = 25$) as a function of baseline assuming normal or inverted mass hierarchy, if the true

TABLE III. Event rates in neutrino mode: The number of signal and background events integrated in reconstructed energy over the first maximum (and second, if possible) for a 175 kt-MW-yr exposure at each baseline in neutrino mode. These rates assume normal hierarchy (inverted hierarchy) and $\delta_{CP} = 0$. (Note that the sensitivities presented in this paper are not based solely on rates, but are calculated by fitting the spectra in bins of reconstructed energy.)

| Baseline (km) | Signal | | Background | | | |
|---------------|------------|-------|------------|--------------|---------------|-----|
| | ν_e CC | Total | ν_e CC | ν_μ CC | ν_τ CC | NC |
| 300 | 752 (532) | 276 | 157 | 75 | 1 | 43 |
| 500 | 692 (504) | 230 | 139 | 45 | 2 | 44 |
| 750 | 738 (470) | 266 | 133 | 60 | 9 | 64 |
| 1000 | 1049 (555) | 392 | 144 | 101 | 37 | 110 |
| 1300 | 1107 (486) | 422 | 146 | 102 | 95 | 79 |
| 1700 | 906 (288) | 330 | 127 | 68 | 92 | 43 |
| 2000 | 1030 (267) | 446 | 114 | 69 | 217 | 46 |
| 2500 | 854 (130) | 331 | 93 | 49 | 164 | 25 |
| 3000 | 844 (77) | 370 | 81 | 38 | 226 | 25 |

TABLE IV. Event rates in antineutrino mode: The number of signal and background events integrated in reconstructed energy over the first maximum (and second, if possible) for a 175 kt-MW-yr exposure at each baseline in antineutrino mode. These rates assume normal hierarchy (inverted hierarchy) and $\delta_{CP} = 0$. (Note that the sensitivities presented in this paper are not based solely on rates, but are calculated by fitting the spectra in bins of reconstructed energy.)

| Baseline (km) | Signal | | Background | | | |
|---------------|----------------------------|-------|----------------------------|--------------------------------|----------------------------------|----|
| | $(\bar{\nu}_e + \nu_e)$ CC | Total | $(\bar{\nu}_e + \nu_e)$ CC | $(\bar{\nu}_\mu + \nu_\mu)$ CC | $(\bar{\nu}_\tau + \nu_\tau)$ CC | NC |
| 300 | 181 (157) | 96 | 46 | 22 | 1 | 27 |
| 500 | 167 (192) | 91 | 49 | 15 | 2 | 25 |
| 750 | 181 (240) | 111 | 50 | 21 | 6 | 34 |
| 1000 | 266 (348) | 186 | 57 | 37 | 30 | 62 |
| 1300 | 243 (378) | 190 | 57 | 37 | 53 | 43 |
| 1700 | 166 (344) | 161 | 53 | 26 | 57 | 25 |
| 2000 | 164 (362) | 201 | 47 | 26 | 104 | 24 |
| 2500 | 112 (331) | 156 | 39 | 19 | 84 | 14 |
| 3000 | 89 (316) | 158 | 31 | 15 | 100 | 12 |

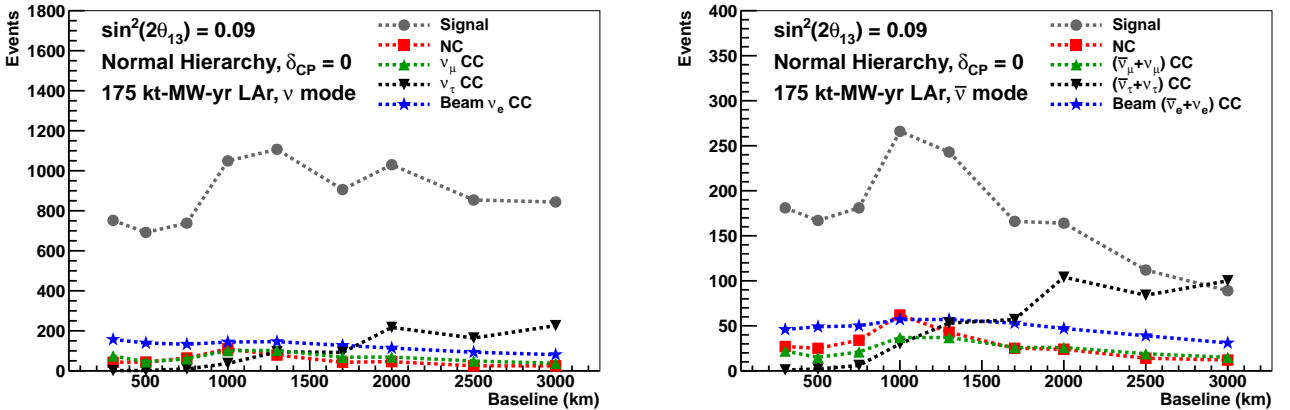


FIG. 11. Event rates vs baseline: The number of signal and background events integrated in reconstructed energy over the first maximum (and second, if possible) for a 175 kt-MW-yr exposure at each baseline in neutrino (left) and antineutrino (right) modes. These rates assume normal hierarchy and $\delta_{CP} = 0$. (Note that the sensitivities presented in this paper are not based solely on rates, but are calculated by fitting the spectra in bins of reconstructed energy.)

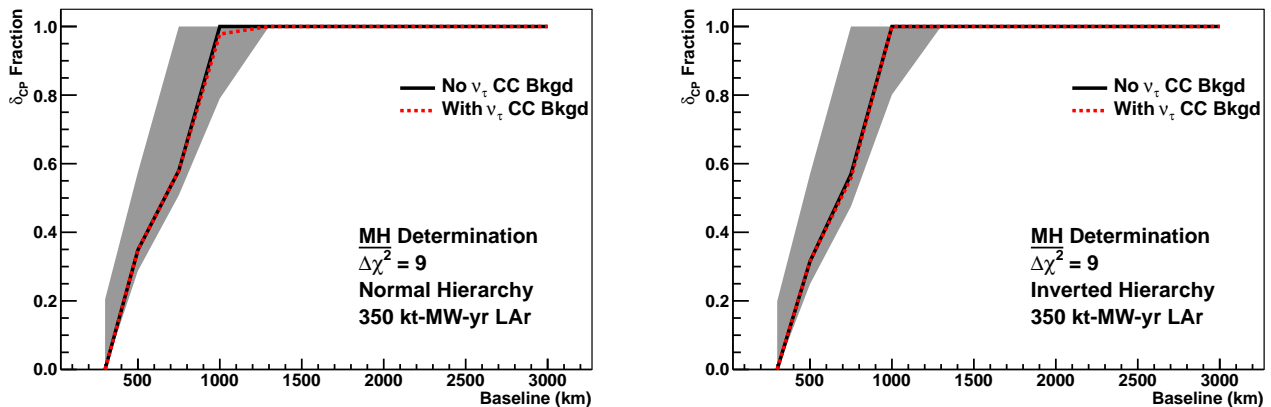


FIG. 12. The fraction of all possible δ_{CP} values for which we can determine normal (left) or inverted (right) mass hierarchy with a minimum value of $\overline{\Delta\chi^2} = 9$ as a function of baseline. An expected average value of $\overline{\Delta\chi^2} = 9$ corresponds to a 93.32% probability of determining the correct mass hierarchy according to the analysis in [34]. The solid black (red dashed) line shows the result including zero (maximum) ν_τ CC background. The shaded band shows the possible range in the fraction due to the uncertainty in the other oscillation parameters and considers both octant solutions for θ_{23} .

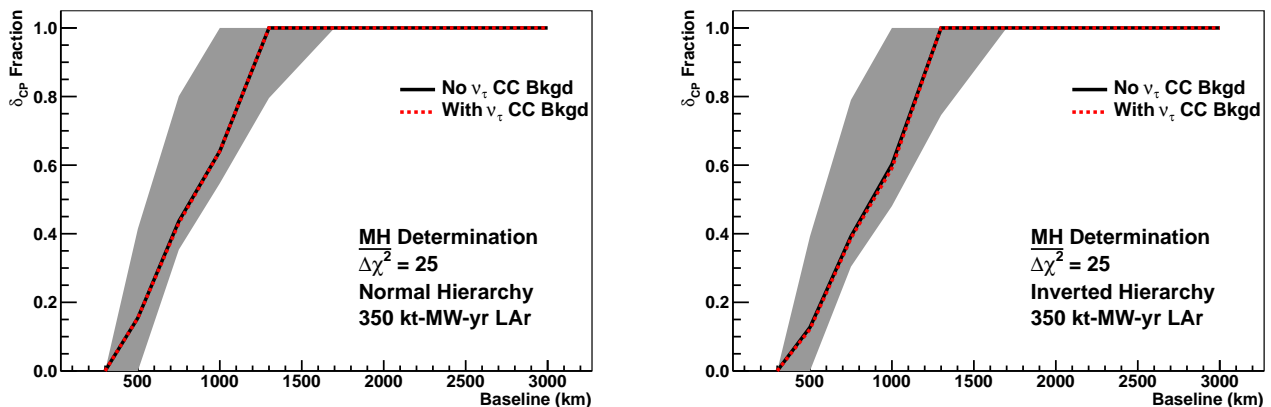


FIG. 13. The fraction of all possible δ_{CP} values for which we can determine normal (left) or inverted (right) mass hierarchy with a minimum value of $\overline{\Delta\chi^2} = 25$ as a function of baseline. An expected average value of $\overline{\Delta\chi^2} = 25$ corresponds to a 99.38% probability of determining the correct mass hierarchy according to the analysis in [34]. The solid black (red dashed) line shows the result including zero (maximum) ν_τ CC background. The shaded band shows the possible range in the fraction due to the uncertainty in the other oscillation parameters and considers both octant solutions for θ_{23} .

value of θ_{23} is within the $1\text{-}\sigma$ allowed region [30]. In these plots we assume that the true hierarchy is unknown by considering both hierarchy solutions in the minimization. We find the octant can be determined at 5σ for 100% of all δ_{CP} values at a baseline of at least 1000 km. We find that the sensitivity at the shortest baselines could increase slightly if the true mass hierarchy is known, but the long baselines still have the best sensitivity.

D. Precision Mixing Angle Measurements

A long-baseline experiment will also make precision measurements of the mixing angles. Figure 25 shows the

resolution of $\sin^2(2\theta_{13})$ as a function of baseline for the nominal exposure of 350 kt-MW-yr. The true mass hierarchy is assumed to be known, and we assume no ν_τ CC background for this calculation. The curves for 100 and 1000 kt-MW-yr exposures are also shown. The best resolution can be achieved at baselines between 1000 and 1500 km.

Figure 26 shows the resolution of $\sin^2\theta_{23}$ as a function of baseline for the nominal exposure of 350 kt-MW-yr. Normal hierarchy is assumed for this calculation, but the choice of hierarchy has negligible impact on this measurement. The curves for 100 and 1000 kt-MW-yr exposures are also shown. The resolution is roughly constant as a function of baseline for baselines 500 km and greater.

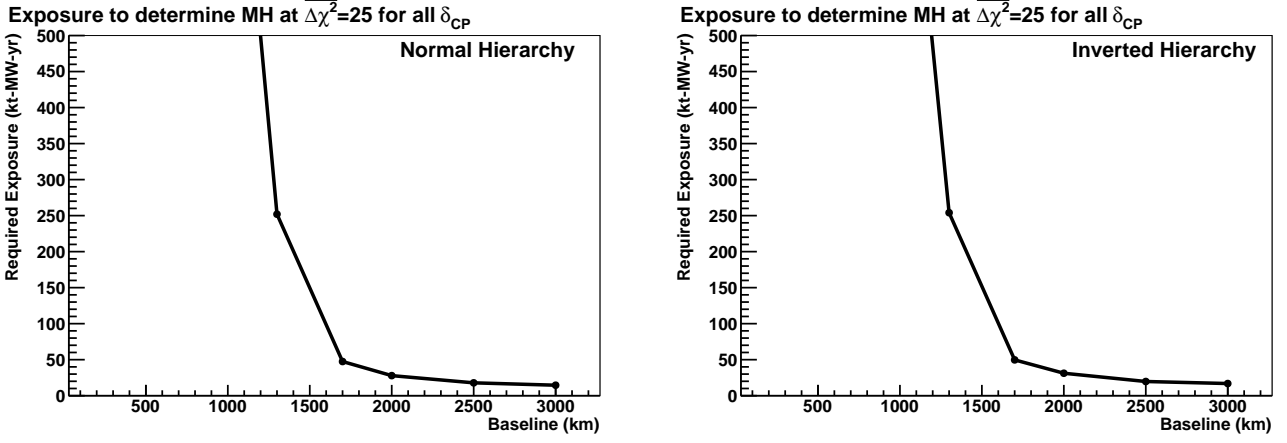


FIG. 14. The exposure required to determine normal(left) or inverted (right) mass hierarchy with a significance of $\overline{\Delta\chi^2} = 25$ for all possible values of δ_{CP} as a function of baseline. We assume no ν_τ CC background.

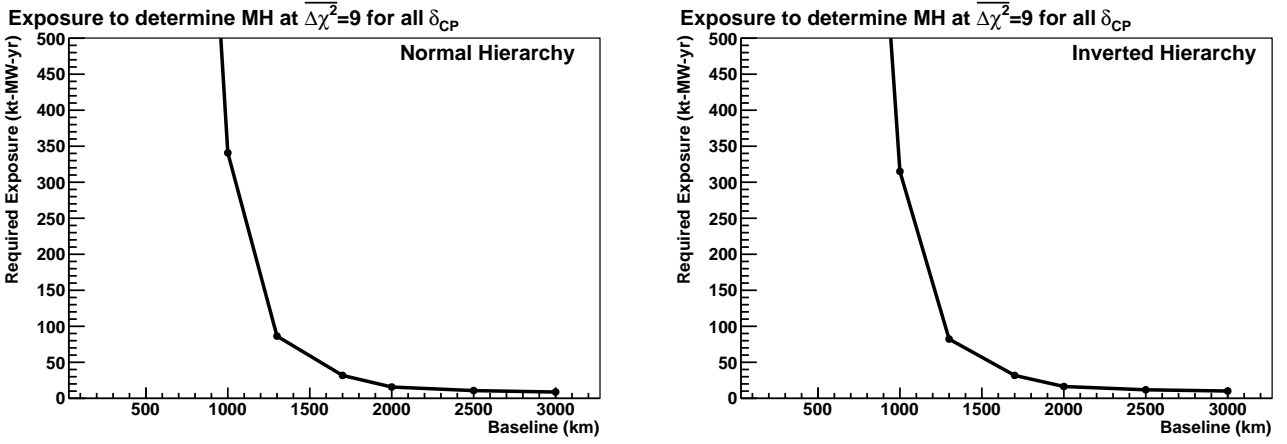


FIG. 15. The exposure required to determine normal(left) or inverted (right) mass hierarchy with a significance of $\overline{\Delta\chi^2} = 9$ for all possible values of δ_{CP} as a function of baseline. We assume no ν_τ CC background.

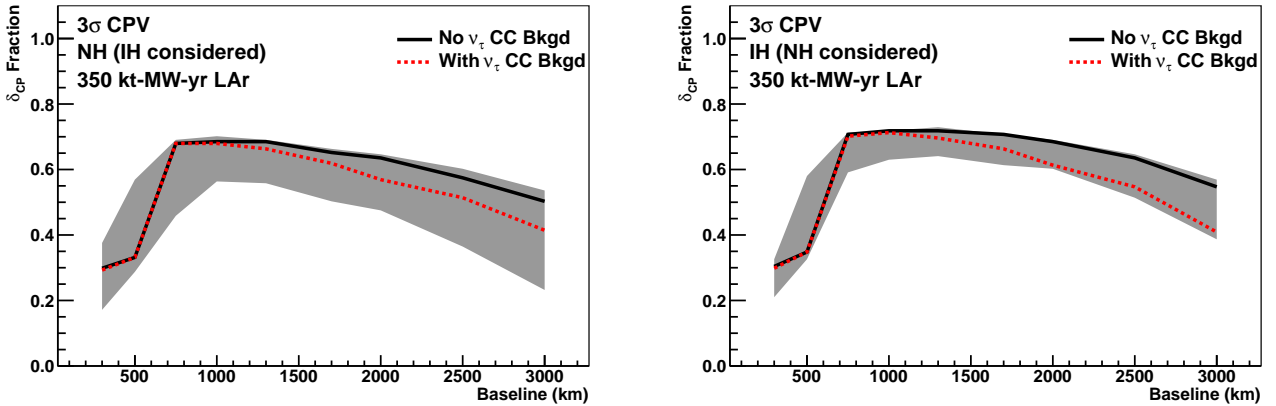


FIG. 16. The fraction of all possible δ_{CP} values for which we can observe CP violation with a sensitivity of at least 3σ ($\Delta\chi^2 = 9$) for normal (left) and inverted (right) mass hierarchy as a function of baseline. The true mass hierarchy is assumed to be unknown. The solid black (red dashed) line shows the result including zero (maximum) ν_τ CC background. The shaded band shows the possible range in the fraction due to the uncertainty in the other oscillation parameters and considers both octant solutions for θ_{23} .

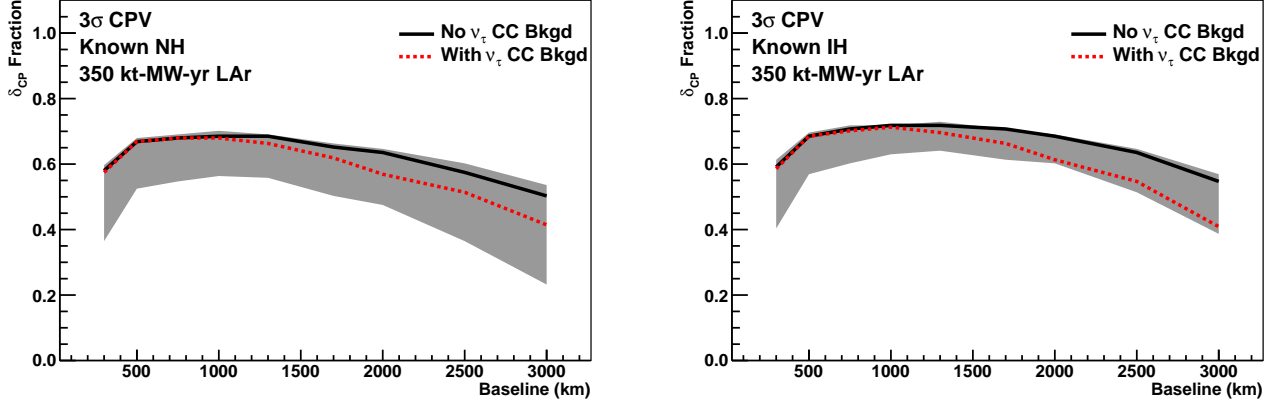


FIG. 17. The fraction of all possible δ_{CP} values for which we can observe CP violation with a sensitivity of at least 3σ ($\Delta\chi^2 = 9$) for normal (left) and inverted (right) mass hierarchy as a function of baseline. The true mass hierarchy is assumed to be perfectly known. The solid black (red dashed) line shows the result including zero (maximum) ν_τ CC background. The shaded band shows the possible range in the fraction due to the uncertainty in the other oscillation parameters and considers both octant solutions for θ_{23} .

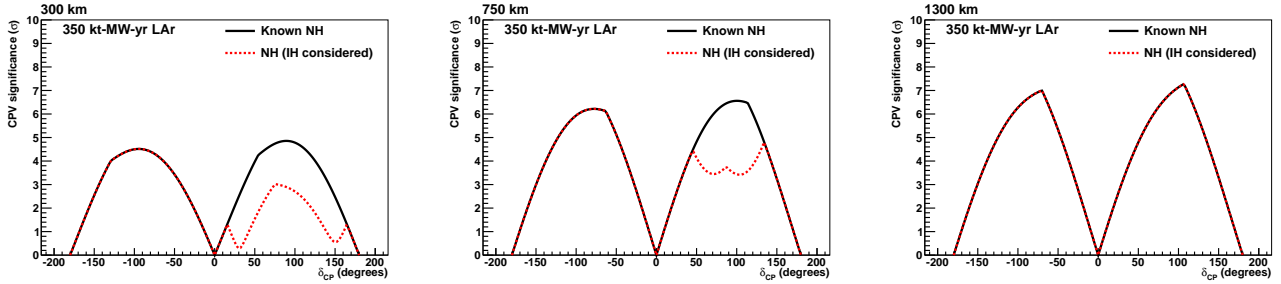


FIG. 18. The significance ($\sigma = \sqrt{\Delta\chi^2}$) at which CP violation can be observed as a function of the true value of δ_{CP} assuming normal hierarchy for 300 km, 750 km, and 1300 km baselines. The significance is shown assuming the hierarchy is perfectly known (black-solid) and assuming both hierarchy solutions are considered (red-dashed). Knowing the hierarchy improves the CP sensitivity at 300 km and 750 km, but has no effect at 1300 km (or baselines > 1300 km).

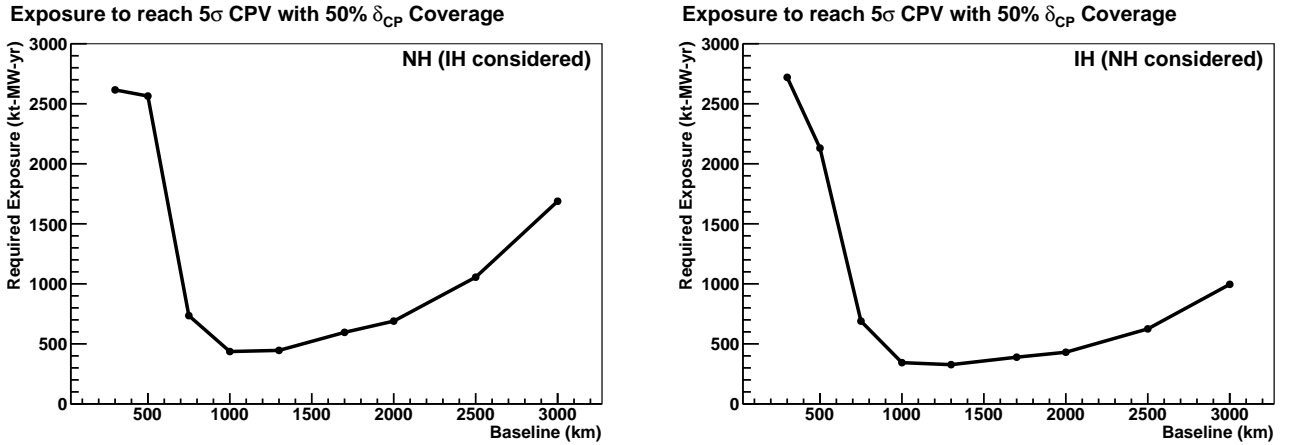


FIG. 19. The exposure required to observe CP violation with a significance of 5σ for 50% of all possible values of δ_{CP} , assuming normal (left) and inverted (right) mass hierarchy, as a function of baseline. The true mass hierarchy is assumed to be unknown, and we assume no ν_τ CC background.

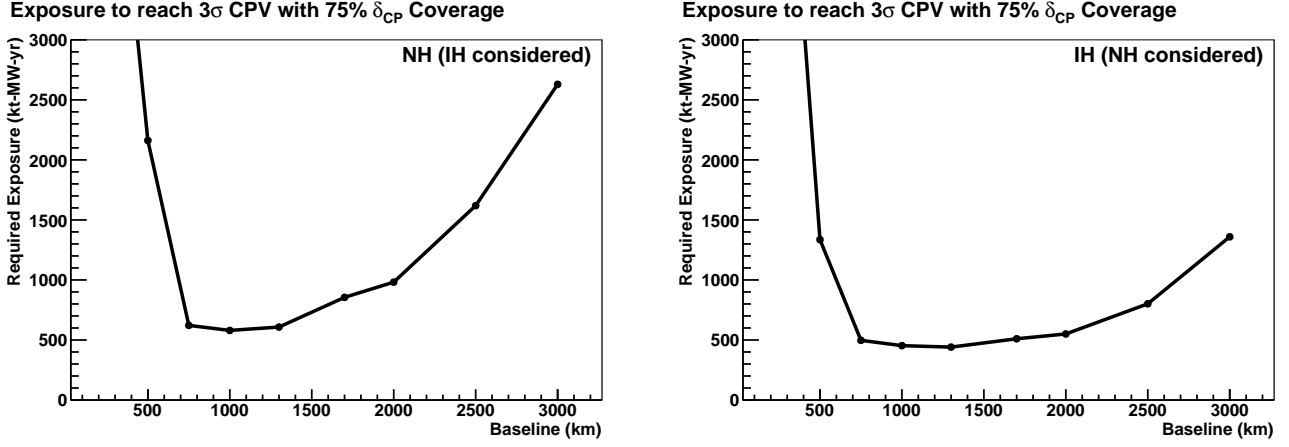


FIG. 20. The exposure required to observe CP violation with a significance of 3σ for 75% of all possible values of δ_{CP} , assuming normal (left) and inverted (right) mass hierarchy, as a function of baseline. The true mass hierarchy is assumed to be unknown, and we assume no ν_τ CC background.

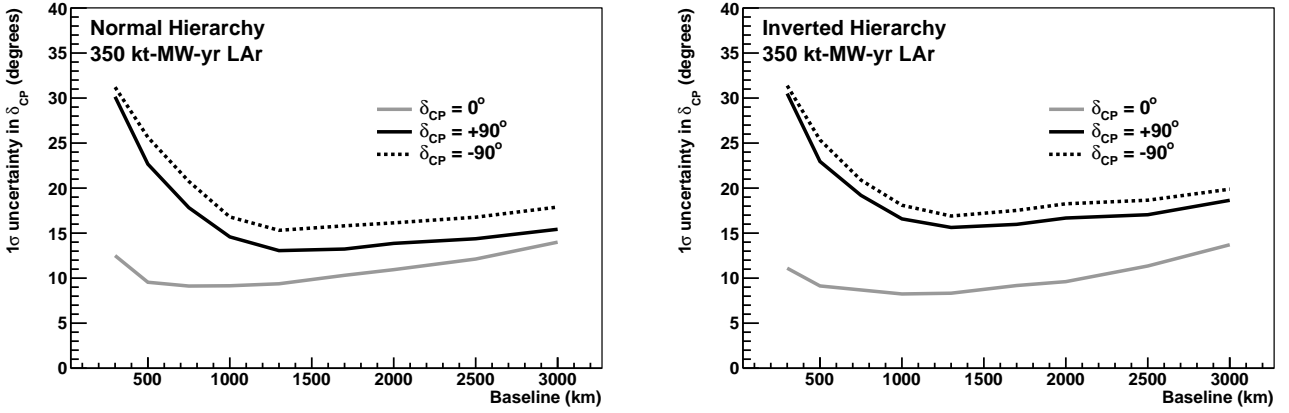


FIG. 21. The 1σ uncertainty in δ_{CP} as a function of baseline assuming the true value of δ_{CP} is 0° (gray solid), $+90^\circ$ (black solid), and -90° (black dashed) for normal (left) and inverted (right) mass hierarchy. The true mass hierarchy is assumed to be perfectly known.

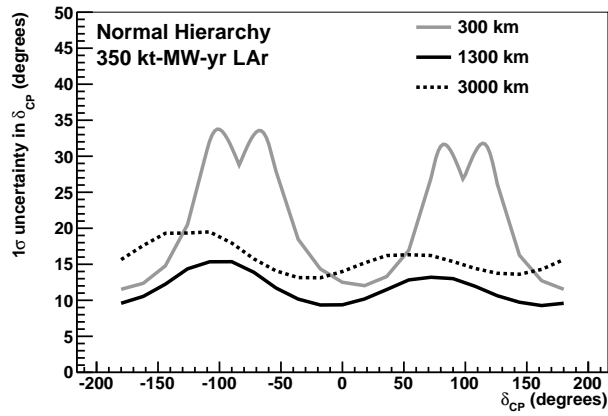


FIG. 22. The 1σ uncertainty in δ_{CP} as a function of the true value of δ_{CP} , assuming the true hierarchy is known to be normal, for baselines of 300 km, 1300 km, and 3000 km.

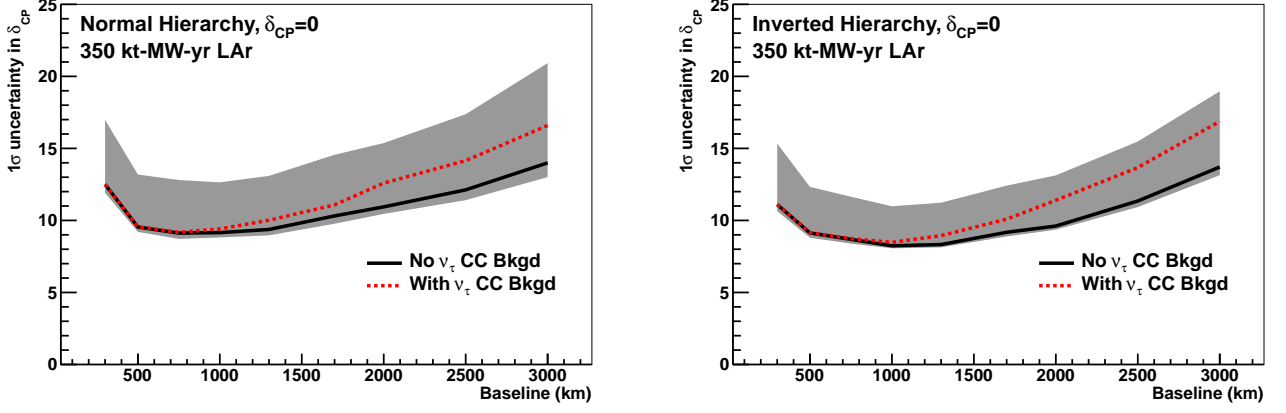


FIG. 23. The 1σ uncertainty in δ_{CP} as a function of baseline, assuming the true value of δ_{CP} is 0° , for normal (left) and inverted (right) mass hierarchy. The true mass hierarchy is assumed to be perfectly known. The solid black (red dashed) line shows the result including zero (maximum) ν_τ CC background. The shaded band shows the possible range in the resolution due to the uncertainty in the other oscillation parameters and considers both octant solutions for θ_{23} .

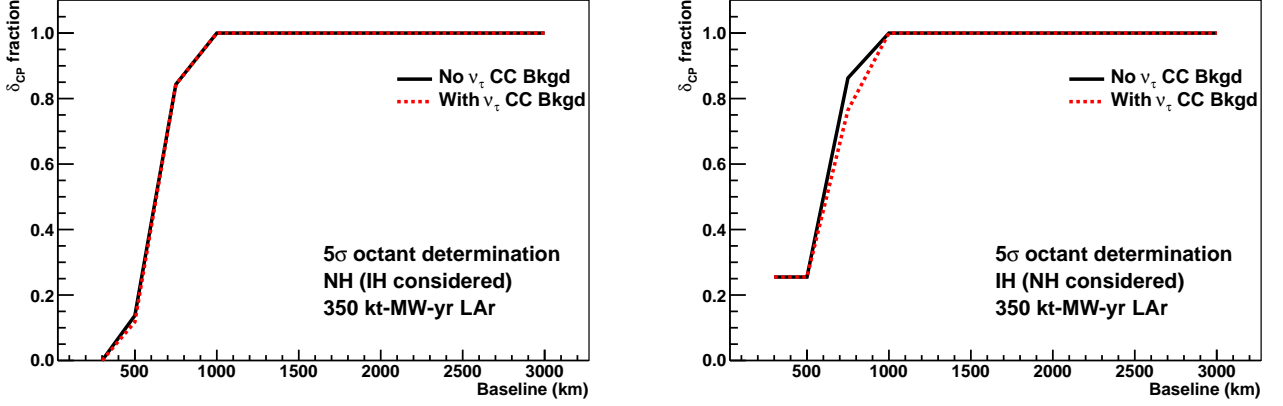


FIG. 24. The fraction of all possible δ_{CP} values for which we can determine the θ_{23} octant with a sensitivity of at least 5σ ($\Delta\chi^2 = 25$) for normal (left) and inverted (right) mass hierarchy as a function of baseline. The true mass hierarchy is assumed to be unknown. The solid black (red dashed) line shows the result including zero (maximum) ν_τ CC background.

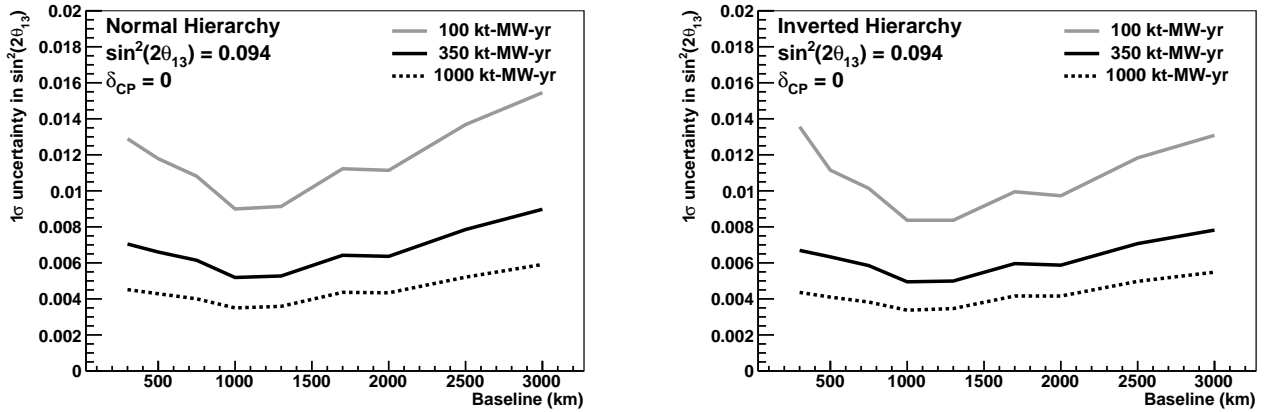


FIG. 25. The 1σ uncertainty in $\sin^2(2\theta_{13})$ as a function of baseline assuming $\sin^2(2\theta_{13}) = 0.094$ and $\delta_{CP} = 0$ for normal (left) and inverted (right) mass hierarchy. The true mass hierarchy is assumed to be perfectly known, and we assume no ν_τ CC background.

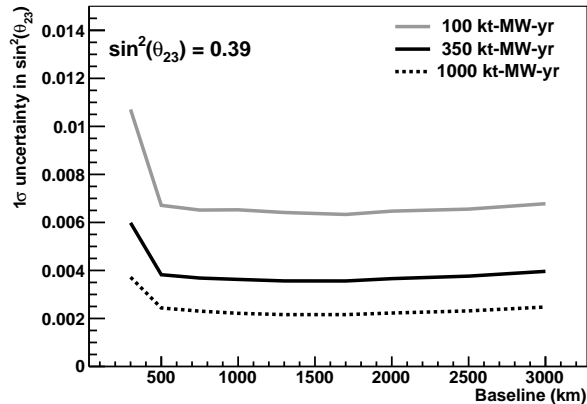


FIG. 26. The 1σ uncertainty in $\sin^2(\theta_{23})$ as a function of baseline assuming $\sin^2(\theta_{23}) = 0.39$.

VI. CONCLUSION

We have studied the sensitivity to the key measurements for an electron neutrino appearance experiment as a function of baseline using a wide-band muon neutrino beam and assuming a nominal exposure of 350 kt-MW-yr. The fluxes are optimized for each baseline considered, assuming achievable beam power and energy from the Fermilab proton complex. We find that a detector at a baseline of at least 1000 km is optimal. In particular, baselines of ~ 1000 -1500 km are optimal to observe CP violation and measure δ_{CP} , the mass hierar-

chy is resolved for all δ_{CP} with $\overline{\Delta\chi^2} = 25$ for baselines greater than 1300 km, and the octant is resolved at 5σ for all δ_{CP} for baselines greater than 1000 km.

ACKNOWLEDGMENTS

We would like to thank Josh Klein, William Louis, Alberto Marchionni, and Michael Mooney for their careful reading and helpful suggestions during the preparation of this manuscript. This material is based upon work supported by the U.S. Department of Energy, Office of Science, Office of High Energy Physics.

-
- [1] R. Wendell *et al.* (Super-Kamiokande Collaboration), Phys.Rev. **D81**, 092004 (2010), arXiv:1002.3471 [hep-ex].
- [2] M. Ahn *et al.* (K2K Collaboration), Phys.Rev. **D74**, 072003 (2006), arXiv:hep-ex/0606032 [hep-ex].
- [3] P. Adamson *et al.* (MINOS Collaboration), Phys. Rev. Lett. **110**, 251801 (2013), arXiv:1304.6335 [hep-ex].
- [4] P. Adamson *et al.* (MINOS Collaboration), Phys.Rev.Lett. **110**, 171801 (2013), arXiv:1301.4581 [hep-ex].
- [5] K. Abe *et al.* (T2K Collaboration), Phys.Rev.Lett. **112**, 181801 (2014), arXiv:1403.1532 [hep-ex].
- [6] K. Abe *et al.* (T2K Collaboration), Phys.Rev.Lett. **112**, 061802 (2014), arXiv:1311.4750 [hep-ex].
- [7] B. Aharmim *et al.* (SNO Collaboration), Phys.Rev. **C81**, 055504 (2010), arXiv:0910.2984 [nucl-ex].
- [8] S. Abe *et al.* (KamLAND Collaboration), Phys.Rev.Lett. **100**, 221803 (2008), arXiv:0801.4589 [hep-ex].
- [9] F. An *et al.* (Daya Bay Collaboration), Phys.Rev.Lett. **112**, 061801 (2014), arXiv:1310.6732 [hep-ex].
- [10] J. Ahn *et al.* (RENO collaboration), Phys.Rev.Lett. **108**, 191802 (2012), arXiv:1204.0626 [hep-ex].
- [11] Y. Abe *et al.* (Double Chooz Collaboration), Phys.Rev. **D86**, 052008 (2012), arXiv:1207.6632 [hep-ex].
- [12] H. Nunokawa, S. J. Parke, and J. W. Valle, Prog.Part.Nucl.Phys. **60**, 338 (2008), arXiv:0710.0554 [hep-ph].
- [13] L. Wolfenstein, Phys.Rev. **D17**, 2369 (1978).
- [14] S. Mikheev and A. Y. Smirnov, Sov.J.Nucl.Phys. **42**, 913 (1985).
- [15] W. Marciano and Z. Parsa, Nucl.Phys.Proc.Suppl. **221**, 166 (2011), arXiv:hep-ph/0610258 [hep-ph].
- [16] M. V. Diwan, Frascati Phys.Ser. **35**, 89 (2004), arXiv:hep-ex/0407047 [hep-ex].
- [17] V. Barger, M. Bishai, D. Bogert, C. Bromberg, A. Curioni, *et al.*, (2007), arXiv:0705.4396 [hep-ph].
- [18] V. Barger, P. Huber, D. Marfatia, and W. Winter, Phys.Rev. **D76**, 053005 (2007), arXiv:hep-ph/0703029 [hep-ph].
- [19] K. Anderson *et al.*, Tech. Rep. FERMILAB-DESIGN-1998-01 (1998).
- [20] R. Brun *et al.*, CERN Program Library Vers. 3.21 W5013 (1993).
- [21] P. Huber, M. Lindner, and W. Winter, Comput.Phys.Commun. **167**, 195 (2005), arXiv:hep-ph/0407333 [hep-ph].
- [22] P. Huber, J. Kopp, M. Lindner, M. Rolinec, and W. Winter, Comput.Phys.Commun. **177**, 432 (2007), arXiv:hep-ph/0701187 [hep-ph].
- [23] A. Ankowski *et al.* (ICARUS Collaboration), Acta Phys.Polon. **B41**, 103 (2010), arXiv:0812.2373 [hep-ex].

- [24] S. Amoruso *et al.* (ICARUS Collaboration), *Eur.Phys.J.* **C33**, 233 (2004), arXiv:hep-ex/0311040 [hep-ex].
- [25] A. Ankowski *et al.* (ICARUS Collaboration), *Eur.Phys.J.* **C48**, 667 (2006), arXiv:hep-ex/0606006 [hep-ex].
- [26] “A Proposal for a Detector 2 km Away from the T2K Neutrino Source,” <http://www.phy.duke.edu/~cwalter/nusag-members/>.
- [27] C. Adams *et al.* (LBNE Collaboration), (2013), arXiv:1307.7335 [hep-ex].
- [28] D. Cherdack, “A Fast MC for LBNE,” <http://meetings.aps.org/link/BAPS.2013.APR.X12.4>, APS April Meeting 2013.
- [29] C. Andreopoulos *et al.*, *Nucl. Instrum. Meth.* **A614**, 87 (2010), arXiv:0905.2517 [hep-ph].
- [30] G. Fogli, E. Lisi, A. Marrone, D. Montanino, A. Palazzo, *et al.*, *Phys.Rev.* **D86**, 013012 (2012), arXiv:1205.5254 [hep-ph].
- [31] F. An *et al.* (Daya Bay Collaboration), *Chin. Phys.* **C37**, 011001 (2013), arXiv:1210.6327 [hep-ex].
- [32] A. M. Dziewonski and D. L. Anderson, *Phys. Earth Planet. Interiors* **25**, 297 (1981).
- [33] F. D. Stacey, *Physics of the earth*, 2nd ed. (Wiley, 1977).
- [34] X. Qian, A. Tan, W. Wang, J. Ling, R. McKeown, *et al.*, *Phys.Rev.* **D86**, 113011 (2012), arXiv:1210.3651 [hep-ph].
- [35] R. Patterson (NOvA Collaboration), *Nucl.Phys.Proc.Suppl.* **235-236**, 151 (2013), arXiv:1209.0716 [hep-ex].
- [36] Y. Wang, “Daya Bay II: A multi-purpose LS-based experiment,” <https://agenda.infn.it/conferenceDisplay.py?confId=5268>, XV International Workshop on Neutrino Telescopes.
- [37] For the measurement of δ_{CP} , there are physical boundaries: $|\sin(\delta_{CP})| < 1$. Therefore, it may not be accurate to determine the 68% confidence interval of δ_{CP} with the simple rule $\Delta\chi^2 = 1$ when the true value of δ_{CP} approaches ± 90 degrees. The actual resolution of δ_{CP} at these values may be slightly better than what is shown in this study. For the purposes of this study, however, it is not crucial.